CCS CHINESE CHEMICAL SOCIETY   PEKING UNIVERSITY 1898   ROYAL SOCIETY OF CHEMISTRY

RESEARCH ARTICLE

Check for updates

Metal–oxide heterointerface synergistic effects of copper–zinc systems for highly selective CO$_2$-to-CH$_4$ electrochemical conversion†

Xingcheng Ma, Dongxu Jiao, Jinchang Fan, Yilong Dong and Xiaoqiang Cui [iD] *

Carbon dioxide (CO$_2$) electrolysis presents a promising route for the conversion of CO$_2$ into value-added products. However, increasing selectivity for a specific deep-reduction product such as methane still remains a great challenge. Here, we report the highly efficient electroreduction of CO$_2$ to methane (CH$_4$) over a precisely controlled Cu–ZnO heterointerface system, which delivered superior activity with a faradaic efficiency of up to 72.4% at −0.7 V *vs.* RHE, surpassing most previously reported catalysts. Experimental measurements and theoretical calculations confirmed the high CO$_2$ to CH$_4$ selectivity was derived from the interfacial synergistic effects between the Cu and ZnO nanostructure. DFT calculations showed that the electronic structure of the interfacial Cu sites was significantly modulated by ZnO, resulting in moderate adsorption energies of *COOH and *CHO intermediates on the Cu sites, in turn, promoting the conversion from CO$_2$ to CH$_4$. This work unravels the strong dependence of CO$_2$-reduction selectivity on the heterointerfaces and provides a platform for designing highly selective electrochemical catalysts.

Introduction

In the context of global warming and combustion of fossil fuels, reducing carbon emissions and upgrading carbon dioxide (CO$_2$) to valued-added commodity chemicals are deemed as key focuses of attention. The CO$_2$ electrolysis process presents a promising route to achieve this goal.[1–6] Among the products in the electrochemical carbon dioxide reduction reaction (CO$_2$RR), methane (CH$_4$) possesses the highest gravimetric energy density (13.9 KW h kg^{-1}) and has attracted considerable attention.[7–9] However, due to the eight-electron transfer process, conversion from CO$_2$ to CH$_4$ still suffers from a large overpotential and low faradaic efficiency (FE).[10] Therefore, developing novel high-efficient (CO$_2$RR) electrocatalysts and uncovering the underlying reaction mechanism is highly desirable.

In this regard, the design of heterostructures is an advanced strategy to achieve favorable catalysis with high selectivity due to their well-defined and closely integrated active sites, which can have a significant influence in the CO$_2$ electrocatalysis, especially for the deep conversion of CO$_2$.[11–17] For example, the tandem catalytic mechanism can be achieved

State Key Laboratory of Automotive Simulation and Control, Key Laboratory of Automobile Materials of MOE and School of Materials Science and Engineering, Jilin University, Changchun, 130012, People's Republic of China.
E-mail: xqcui@jlu.edu.cn
†Electronic supplementary information (ESI) available. See DOI: https://doi.org/10.1039/d2qi02051c

by introducing Ag or Au on Cu sites, where the CO$_2$ conversion to CO occurs on the Ag or Au sites and the C–C bond formation step occurs on the Cu sites, generating various products including *n*-propanol, propionaldehyde, and ethanol.[18,19] The tailored introduction of Ag can also optimize the coordinated number and oxide state of surface Cu sites, promoting suitable *CO adsorption for the C–C coupling process.[20,21] These studies prove the potential of utilizing heterointerfaces to adjust the adsorption of critical intermediates and driving the reaction to proceed to the expected pathway; however, high CO$_2$–CH$_4$ conversion activity based on heterostructure catalysts has rarely been reported.

Here, we synthesized a series of Cu–ZnO heterostructure catalysts with a tunable ratio of heterointerfaces as efficient electrocatalysts for CO$_2$ reduction. Cu was used to provide the active sites[22,23] and ZnO was used to assist in the deep conversion of carbon dioxide.[24–26] Therefore, in this work, by precisely adjusting the heterointerface ratio between Cu and ZnO, the highly selective conversion of CO$_2$ to CH$_4$ was achieved with a faradaic efficiency of 72.4% at −0.7 V *vs.* RHE, outperforming most reported catalysts. Further investigations based on experimental measurements and theoretical calculations indicated that the outstanding CO$_2$–CH$_4$ performance was derived from the interfacial synergistic effect between Cu and ZnO. Due to the modulation of ZnO, the d-band center of the interfacial Cu sites were upshifted, which increased the adsorption energies of the *COOH and *CHO intermediates on the interfacial Cu sites, which in turn promoted the conversion from CO$_2$ to CH$_4$.

Experimental section

Synthesis of different Cu : Zn ratios of Cu–ZnO catalysts

First, 0.5 g of copper nitrate and 0.5 g zinc nitrate were put in a 50 mL beaker. Next, 5 mL of deionized water was used to dissolve the metal salts. Then, 0.5 g of tissue paper processed by a shredder was added in the metal salt solution and the hybrid materials were stirred and sonicated until the solution was completely adsorbed on the finely crumbled paper. The mixture was then heated at 80 °C for several hours to dry thoroughly. Afterward, the mixture was annealed using a tube furnace at 700 °C under a high-purity argon atmosphere for 3 h with a 5 °C min⁻¹ heating rate. It was noted that high-purity argon gas should be kept continuously to remove unnecessary air for at least 2 h before the annealing process to avoid explosion. The resulting product was denoted as 2Cu–1ZnO. The product was kept in a centrifuge tube for further use. Also, 9Cu–1ZnO, 4Cu–1ZnO, and 1Cu–1ZnO electrocatalysts were prepared by tuning the feed ratio of copper/zinc salt at ratios of 0.8/0.2, 0.67/0.33, and 0.2 g/0.8 g, respectively. As controls, following the similar procedure, Cu–Cu$_2$O and ZnO electrocatalysts were synthesized with only 1.0 g copper or 1.0 g zinc salt used in the experimental process.

Synthesis of Cu–ZnO with different amounts of substrate

Electrocatalysts with different metal salt : tissue paper ratios (3 : 1, 1 : 1, and 0.5 : 1) were also prepared by adjusting the feed ratio of copper/zinc salt at 0.75/0.75, 0.25/0.25, and 0.125 g/0.125 g, respectively. Afterward, the electrocatalysts were synthesized following the same procedure as mentioned below.

For more information, see details in the ESI.†

Results and discussion

Schematic diagrams of the designed heterointerface structures are shown in Fig. 1a, where the red ball is Cu covered by green ZnO. By adjusting the feed amount of copper and zinc sources, the coverage could be modulated. This variation in the exposed interfaces resulted in different CO$_2$RR products changing from CO to CH$_4$. The Cu–ZnO electrocatalysts were synthesized *via* a process of carbonizing tissue paper with the adsorption of different metal ion feed ratios. The structure details of the resulting Cu–ZnO samples obtained by SEM and EDX-mapping tests are shown in Fig. 1b and c, which clearly exhibited the heterostructures with different ZnO coverage rates. The atomic ratios of Cu : Zn were measured to be of 9 : 1, 4 : 1, 2 : 1, and 1 : 1 by inductively coupled plasma mass spectrometry (ICP-MS). Cu structures (red areas) were covered by ZnO nanoparticles (green areas), exposing abundant Cu–ZnO heterointerfaces. Zn and O had similar distributions and Cu exhibited complementary patterns (Fig. S1†). The coverage of ZnO on copper surfaces was changed with the atomic ratio of Cu : Zn, and 2Cu–1ZnO exhibited the most heterointerfaces. For comparison, catalysts with different amounts of metal ions and tissue paper were prepared in the experiment (Fig. S2 and
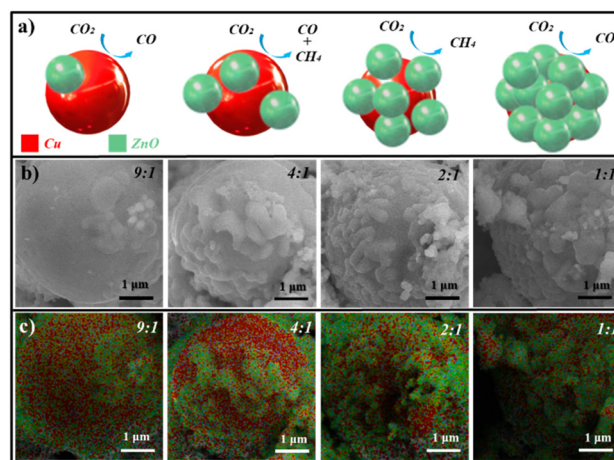

Fig. 1 (a) Schematic diagrams of the designed heterointerface structures. Red and green balls represent metal Cu and ZnO, respectively. (b) SEM images and (c) overlap mapping pictures of the Cu-ZnO catalysts with different heterointerfaces. The Cu : Zn ratios were 9 : 1, 4 : 1, 2 : 1, and 1 : 1, respectively. Red and green areas represent the element distribution of Cu and Zn, respectively. The ratios were acquired from ICP tests.

S3†), and distinct morphologies were acquired. In addition, too much tissue paper did not lead to the formation of heterostructures, but generated nanoparticles in the carbon matrices.[27] The X-ray diffraction (XRD) patterns of the Cu–ZnO catalysts were characterized and analyzed as shown in Fig. 2a. All the Cu–ZnO catalysts possessed a clear two-phase heterostructure, which could be ascribed to metallic Cu (black standard line, JCPDS: 04-0836) and ZnO (red standard line, JCPDS: 36-1451), but exhibited different relative strengths of XRD peaks (Fig. 2b). The structure with Cu$_2$O on the Cu surface could be acquired without zinc sources according to the Cu$_2$O PDF standard card (JCPDS: 05-0667). Also, the pure ZnO structure could be obtained without copper sources (Fig. S4†). In addition, Cu–ZnO catalysts with different feed ratios of metal ions and tissue paper were also characterized (Fig. S5†), in which the phases of Cu and ZnO could also be observed in the diffraction patterns. The relative intensity of the diffraction peaks decreased with the reduced feed ratios of metal ions, which agreed well with the SEM and SEM-mapping observations mentioned above. Fig. 2b shows the HRTEM image of 2Cu–1ZnO electrocatalysts, together with patterns derived from the yellow and blue areas. The heterointerface can be clearly observed, marked by the red dotted line. The nanostructure showed (111) facets of metallic Cu with a lattice parameter of 2.1 Å (Fig. 2c), and (002) facets of ZnO with a lattice parameter of 2.6 Å (Fig. 2d). The formed nanostructure clearly indicated the formation of heterogeneous Cu–ZnO.

X-Ray photoelectron spectroscopy (XPS) was further used to analyze the surface components of Cu–ZnO catalysts with different heterointerfaces. The Zn 2p spectrum was detected and is shown in Fig. 2e. The peaks of Zn^{2+} were shifted to higher energy with the increased Zn content of the catalysts.
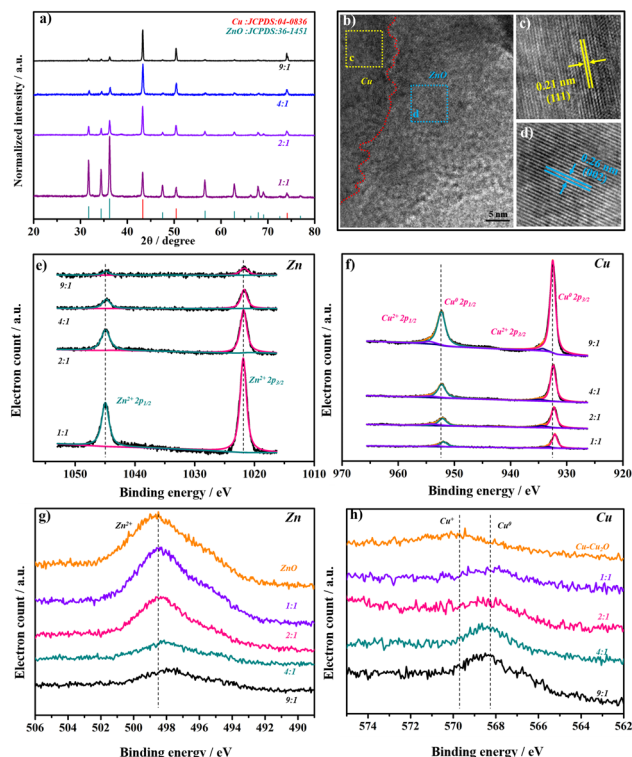
Fig. 2 (a) XRD patterns of different Cu : Zn ratios of Cu–ZnO catalysts. (b) HRTEM of 2Cu–1ZnO, together with patterns derived from the (c) yellow and (d) blue areas. XPS spectra of the selected samples: (e) Zn 2p, (f) Cu 2p, (g) Zn Auger peaks, and (h) Cu Auger peaks, respectively.

Fig. 3 (a) Linear sweep voltammetry curves, (b) CH_4 faradaic efficiency, (c) CO faradaic efficiency, and (d) H_2 faradaic efficiency of Cu powder, Cu–Cu$_2$O, ZnO, and Cu–ZnO with different Cu : Zn ratios. (e) CH_4 partial current density of different catalysts. (f) Relationship between the performance, components, and morphology of Cu–ZnO catalysts.

ZnO also showed the same tendency (Fig. S6†). The shifts of the Cu peaks were opposite to those of Zn, decreasing from 9 : 1 to 1 : 1. These XPS results indicated there were electronic interactions between Cu and Zn, especially when the ratio between Cu and Zn became larger, where the shifts seemed more obvious. Compared with 1Cu–1ZnO catalyst, 2Cu–1ZnO had rather smaller shifts (−0.06 eV for Zn and +0.07 eV for Cu). At the same time, 9Cu–1ZnO changed more clearly (−0.12 eV for Zn and +0.35 eV for Cu, also compared with 1Cu–1ZnO). Furthermore, the Zn and Cu auger spectra were also detected to distinguish Cu^0/Cu^+ and Zn^0/Zn^{2+}, indicating the presence of the Zn^{2+} and Cu^0 species of Cu–ZnO catalysts (Fig. 2g and h).[12,28]

The electrochemical properties of Cu–ZnO and related catalysts were studied by electrochemical tests in a gas-tight three-electrode H-type cell with 0.1 M KHCO$_3$ solution, which was CO_2-saturated. The details are shown in the Experimental section and the results are shown in Fig. 3. As shown in Fig. 3a, the linear sweep voltammetry (LSV) curves showed that the ZnO and Cu–ZnO catalysts had better current densities for the electrochemical reduction process, compared with Cu powder and Cu–Cu$_2$O catalysts. Among the Cu–ZnO catalysts, 2Cu–1ZnO exhibited the best electrochemical activity with the smallest overpotential and the largest current density. To further quantify the CO_2RR performance of different catalysts, the faradaic efficiency (FE) was evaluated by using nuclear
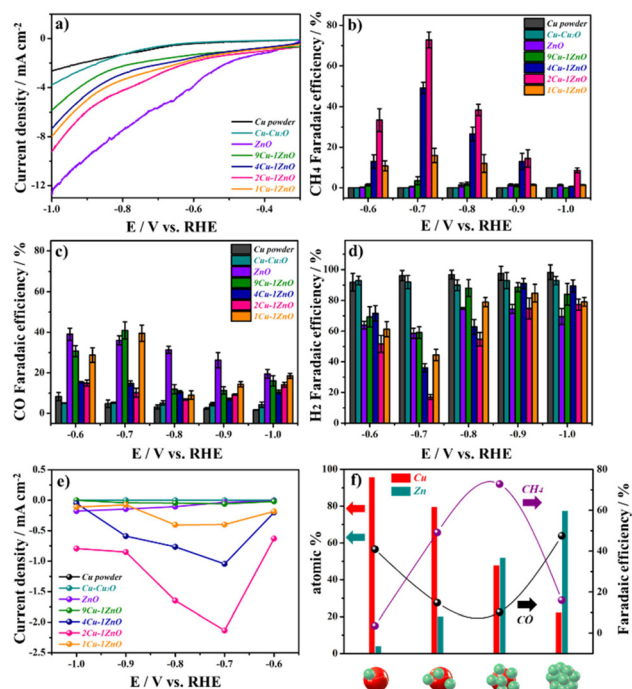
magnetic resonance (for liquid products) analyses and gas chromatography (for gas products).The FE_{CH_4} of 2Cu–1ZnO reached 72.4% at −0.7 V *vs.* RHE in CO_2-saturated electrolyte (Fig. 3b), which exhibited good performances among Cu-based catalysts (Tables S1 and S2†). Although the ZnO catalyst exhibited the best current density, the major reduction products were CO (Fig. 3c) and H_2 (Fig. 3d), while only a few CH_4 could be detected in this condition. Also, 4Cu–1ZnO exhibited good a FE_{CH_4} (49.1%). However, 9Cu–1ZnO and 1Cu–1ZnO showed poor selectivities for CH_4, only 3.5% and 16%, respectively. By contrast, their selectivities for CO and H_2 remained dominant. The partial current density of different products revealed the same results. 2Cu–1ZnO showed the best selectivity and a high yield of CH_4 (Fig. 3e). At the same time, the CO and H_2 yields of 2Cu–1ZnO underperformed the other catalysts (Fig. S7 and S8†). To better gauge the CO_2RR properties of the Cu–ZnO heterostructure, we also analyzed the catalysts with different feed ratios of metal ions and tissue paper, and found that catalysts without a suitable heterostructure had an obviously reduced selectivity for CH_4 as well (Fig. S9†). These electrochemical results indicated the relationship between the structure and performance, whereby CH_4 could be generated with Cu–ZnO catalysts with a suitable heterostructure. The surface content of Cu–ZnO catalysts could be summarized by integrating the peak areas according to XPS in Fig. 2e and f. When the Cu : Zn ratio was close to 1 : 1, the selectivity for CH_4 was excellent in our tests (Fig. 3f). These results indicate that the cover-

170 | *Inorg. Chem. Front.*, 2023, **10**, 168–173

This journal is © the Partner Organisations 2023

age of ZnO on the Cu surface influences the performance. Suitable heterostructures are important for the CO_2RR. The stability of 2Cu–1ZnO was tested at −0.7 V *vs.* RHE (Fig. S10†), and exhibited good stability. Also, the 2Cu–1ZnO catalyst showed similar structures before and after the electrochemical tests, indicating its satisfactory structural stability (Fig. S11 and S12†).

DFT calculations were performed to study the reasons for the good performance observed on the 2Cu–1ZnO catalyst. The optimized simulated geometries for the CO_2RR reaction steps are shown in Fig. 4a. The chemical bonding between parts of Cu and ZnO could be verified by the sliced electron localization function (ELF) maps. According to the results, there were covalent bonds between Cu and O and Zn and O. Also, there may be metallic bonds between Cu and Zn (Fig. S13†).[29,30] The Gibbs free energy (ΔG) values of the potential-limiting step (PDS) for the CO_2RR on these catalysts were used to explain the experimental results. The free energy diagrams for CO_2–CH_4 are summarized in Fig. 4b. Here, *CHO species is one of the most critical intermediates for CH_4 generation. The ability for intermediate adsorption always influences the performances.[31,32] The specific CO_2-to-CH_4 reaction pathway was: * → *COOH → *CO → *CHO → *CH$_2$O → *CH$_3$O → *O → *OH → * (where * represents the catalytic site). The ΔG value

of *CHO on the Cu–ZnO was 0.52 eV, which was the smallest among the catalysts. Furthermore, compared with the energy barrier for *CO → *CHO, Cu needs more energy to go from *COOH → *CO (1.13 eV) and ZnO needs more to go from *OH → * (1.06 eV), respectively. These results indicate that the catalytic activity of Cu–ZnO for the electrochemical CO_2 to CH_4 could be expected to be improved, which could be ascribed to the enhanced adsorption with the *CHO species. The ΔG value of COOH* on ZnO was 0.71 eV along the CO pathway, which was smaller by approximately 0.04 eV and 0.42 eV than that on Cu-ZnO and pristine Cu, respectively (Fig. 4c). Considering the energy barrier for the CH_4 generation, ZnO is more likely to generate CO, which is consistent with the experimental phenomenon. As shown in Fig. 4d, we found that the ΔG_{H*} value for HER on Cu–ZnO was approximately −0.58 eV, which was further away from 0 eV than the values of −0.24 eV on the ZnO and 0.19 eV on the Cu, respectively. Therefore, Cu–ZnO could be expected to have poor HER catalytic activity. Meanwhile, the formation of H_2 for the Cu–ZnO system needed a higher energy barrier of 1.12 eV (Fig. S14†), indicating that CH_4 species were more accessible to obtain on the heterointerface. These results can be understood in terms of the electronic structure. The D-band center (ε_d) is consistent with the CO_2RR catalytic activity. The closer the d-band center is to the Fermi level, the stronger the adsorption, within the d-band center theory.[33] Designing heterointerface electrochemical catalysts with a suitable d-band center for the generation of specific products by interfacial synergistic effect is very promising. Our results show that when ε_d shifted closer to the Fermi energy level (from −2.34 eV to −2.17 eV), less free energy was required to generate the intermediates of *COOH and *CHO, indicating the enhanced CH_4 catalytic activity of the Cu–ZnO heterostructures (Fig. 4e and f).
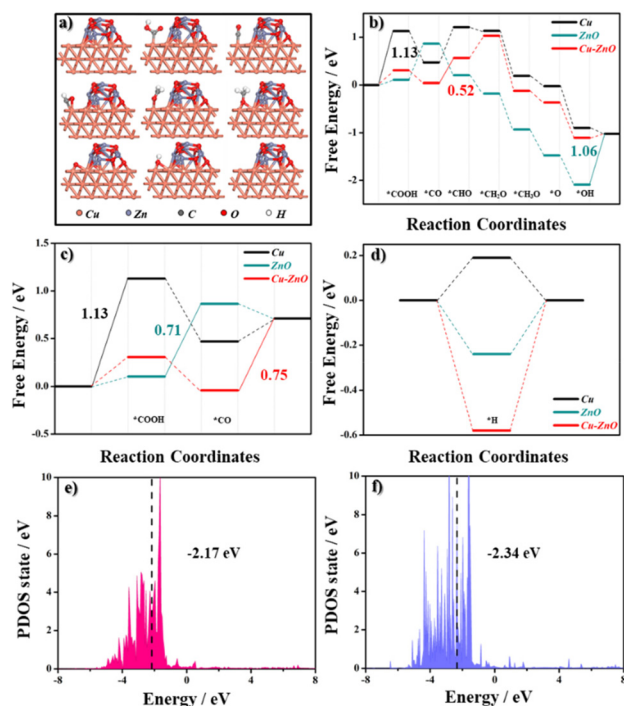
Conclusions

In summary, we report the synthesis of heterointerface catalysts with Cu–ZnO interfacial sites *via* a carbonization process. The resulting heterogeneous structure of Cu–ZnO promoted CO_2 reduction to CH_4. The experimental results and theoretical calculations showed that the high performance could be attributed to the synergy between ZnO and Cu. This work unravels the strong dependence of carbon dioxide reduction selectivity on the heterogeneous catalysts, and provides a platform for designing highly selective electrochemical catalysts.

Conflicts of interest

There are no conflicts to declare.

Acknowledgements

Fig. 4 DFT-optimized geometries for CO_2 conversion to CH_4 on the Cu–ZnO heterostructure. (a) The model of the Cu–ZnO heterostructure. The involved CO_2RR reaction intermediate steps on Cu–ZnO. Orange, white, red, gray, and blue balls represent Cu, H, O, C, and Zn, respectively. Free energy diagrams for CO_2 reduction into (b) CH_4, (c) CO, and (d) H_2 on Cu, ZnO, and Cu–ZnO heterostructure. Calculated partial density of states (PDOS) of Cu site of (e) Cu–ZnO and (f) Cu, where the black line presents the d-band center.

This journal is © the Partner Organisations 2023

Inorg. Chem. Front., 2023, **10**, 168–173 | **171**

References

1 R. G. Mariano, M. Kang, O. J. Wahab, I. J. McPherson, J. A. Rabinowitz, P. R. Unwin and M. W. Kanan, Microstructural origin of locally enhanced CO_2 electrore-duction activity on gold, *Nat. Mater.*, 2021, **20**, 1000–1006.

2 C. Kim, J. C. Bui, X. Luo, J. K. Cooper, A. Kusoglu, A. Z. Weber and A. T. Bell, Tailored catalyst microenvironments for CO_2 electroreduction to multicarbon products on copper using bilayer ionomer coatings, *Nat. Energy*, 2021, **6**, 1026–1034.

3 B. Endrodi, A. Samu, E. Kecsenovity, T. Halmagyi, D. Sebok and C. Janaky, Operando cathode activation with alkali metal cations for high current density operation of water-fed zero-gap carbon dioxide electrolyzers, *Nat. Energy*, 2021, **6**, 439–448.

4 S. Jin, Z. Hao, K. Zhang, Z. Yan and J. Chen, Advances and challenges for the electrochemical reduction of CO_2 to CO: From fundamentals to industrialization, *Angew. Chem.*, 2021, **133**, 20627–20648.

5 H. Guo, D. Si, H. Zhu, Q. Li, Y. Huang and R. Cao, Ni single-atom sites supported on carbon aerogel for highly efficient electroreduction of carbon dioxide with industrial current densities, *eScience*, 2022, **2**, 295–303.

6 J. Albo, D. Vallejo, G. Beobide, O. Castillo, P. Castaño and A. Irabien, Copper-based metal-organic porous materials for CO_2 electrocatalytic reduction to alcohols, *ChemSusChem*, 2017, **10**, 1100–1109.

7 C. Steinlechner and H. Junge, Renewable methane generation from carbon dioxide and sunlight, *Angew. Chem., Int. Ed.*, 2018, **57**, 44–45.

8 L. Zhang, X. X. Li, Z. L. Lang, Y. Liu, J. Liu, L. Yuan, W. Y. Lu, Y. S. Xia, L. Z. Dong, D. Q. Yuan and Y. Q. Lan, Enhanced cuprophilic interactions in crystalline catalysts facilitate the highly selective electroreduction of CO_2 to CH_4, *J. Am. Chem. Soc.*, 2021, **143**, 3808–3816.

9 Z. Chen, M.-R. Gao, Y.-Q. Zhang, N. Duan, T. Fan, J. Xiao, J. Zhang, Y. Dong, J. Li, X. Yi and J.-L. Luo, Tuning local carbon active sites saturability of graphitic carbon nitride to boost CO_2 electroreduction towards CH_4, *Nano Energy*, 2020, **73**, 104833.

10 Z. W. Seh, J. Kibsgaard, C. F. Dickens, I. Chorkendorff, J. K. Norskov and T. F. Jaramillo, Combining theory and experiment in electrocatalysis: Insights into materials design, *Science*, 2017, **355**, eaad4998.

11 Q. Fan, M. Zhang, M. Jia, S. Liu, J. Qiu and Z. Sun, Electrochemical CO_2 reduction to C_{2+} species: Heterogeneous electrocatalysts, reaction pathways, and optimization strategies, *Mater. Today Energy*, 2018, **10**, 280–301.

12 J. Zeng, T. Rino, K. Bejtka, M. Castellino, A. Sacco, M. A. Farkhondehfal, A. Chiodoni, F. Drago and C. F. Pirri, Coupled copper-zinc catalysts for electrochemical reduction of carbon dioxide, *ChemSusChem*, 2020, **13**, 4128–4139.

13 Z. Li, R. M. Yadav, L. Sun, T. Zhang, J. Zhang, P. M. Ajayan and J. Wu, CuO/ZnO/C electrocatalysts for CO_2-to-C_{2+} products conversion with high yield: On the effect of geometric structure and composition, *Appl. Catal., A*, 2020, **606**, 117829.

14 D. Ren, J. Gao, L. Pan, Z. Wang, J. Luo, S. M. Zakeeruddin, A. Hagfeldt and M. Gratzel, Atomic layer deposition of ZnO on CuO enables selective and efficient electroreduction of carbon dioxide to liquid fuels, *Angew. Chem., Int. Ed.*, 2019, **58**, 15036–15040.

15 S. B. Varandili, J. Huang, E. Oveisi, G. L. De Gregorio, M. Mensi, M. Strach, J. Vavra, C. Gadiyar, A. Bhowmik and R. Buonsanti, Synthesis of Cu/CeO_{2-x} nanocrystalline het-erodimers with interfacial active sites to promote CO_2 elec-troreduction, *ACS Catal.*, 2019, **9**, 5035–5046.

16 C. Choi, J. Cai, C. Lee, H. M. Lee, M. Xu and Y. Huang, Intimate atomic Cu-Ag interfaces for high CO_2RR selectivity towards CH_4 at low over potential, *Nano Res.*, 2021, **14**, 3497–3501.

17 I. Merino-Garcia, J. Albo, J. Solla-Gullón, V. Montiel and A. Irabien, Cu oxide/ZnO-based surfaces for a selective ethylene production from gas-phase CO_2 electroconversion, *J. CO_2 Util.*, 2019, **31**, 135–142.

18 P. B. O'Mara, P. Wilde, T. M. Benedetti, C. Andronescu, S. Cheong, J. J. Gooding, R. D. Tilley and W. Schuhmann, Cascade reactions in nanozymes: spatially separated active sites inside Ag-core-porous-Cu-shell nanoparticles for mul-tistep carbon dioxide reduction to higher organic mole-cules, *J. Am. Chem. Soc.*, 2019, **141**, 14093–14097.

19 C. G. Morales-Guio, E. R. Cave, S. A. Nitopi, J. T. Feaster, L. Wang, K. P. Kuhl, A. Jackson, N. C. Johnson, D. N. Abram, T. Hatsukade, C. Hahn and T. F. Jaramillo, Improved CO_2 reduction activity towards C_{2+} alcohols on a tandem gold on copper electrocatalyst, *Nat. Catal.*, 2018, **1**, 764–771.

20 P. Wang, H. Yang, C. Tang, Y. Wu, Y. Zheng, T. Cheng, K. Davey, X. Huang and S. Z. Qiao, Boosting electrocatalytic CO_2-to-ethanol production via asymmetric C-C coupling, *Nat. Commun.*, 2022, **13**, 3754.

21 X. Ma, F. Wang, D. Jiao, D. Zhang, X. Zhao, D. J. Singh, J. Zhao, X. Cui and W. Zheng, Room-temperature liquid metal synthesis of nanoporous copper-indium hetero-structures for efficient carbon dioxide reduction to syngas, *Sci. China Mater.*, 2022, 1–9.

22 I. Merino-Garcia, J. Albo and A. Irabien, Tailoring gas-phase CO_2 electroreduction selectivity to hydrocarbons at Cu nanoparticles, *Nanotechnology*, 2018, **29**, 014001.

23 I. Merino-Garcia, J. Albo and A. Irabien, Productivity and selectivity of gas-phase CO_2 electroreduction to methane at

172 | *Inorg. Chem. Front.*, 2023, **10**, 168–173

This journal is © the Partner Organisations 2023

copper nanoparticle-based electrodes, *Energy Technol.*, 2017, **5**, 922–928.

24 J. Albo, A. Sáez, J. Solla-Gullón, V. Montiel and A. Irabien, Production of methanol from CO_2 electroreduction at Cu_2O and Cu_2O/ZnO-based electrodes in aqueous solution, *Appl. Catal., B*, 2015, **176–177**, 709–717.

25 R. A. Geioushy, M. M. Khaled, K. Alhooshani, A. S. Hakeem and A. Rinaldi, Graphene/ZnO/Cu_2O electrocatalyst for selective conversion of CO_2 into *n*-propanol, *Electrochim. Acta*, 2017, **245**, 456–462.

26 J. Albo and A. Irabien, Cu_2O-loaded gas diffusion electrodes for the continuous electrochemical reduction of CO_2 to methanol, *J. Catal.*, 2016, **343**, 232–239.

27 M. A. Ahsan, A. R. P. Santiago, Y. Hong, N. Zhang, M. Cano, E. Rodriguez-Castellon, L. Echegoyen, S. T. Sreenivasan and J. C. Noveron, Tuning of trifunctional NiCu bimetallic nanoparticles confined in a porous carbon network with surface composition and local structural distortions for the electrocatalytic oxygen reduction, oxygen and hydrogen evolution reactions, *J. Am. Chem. Soc.*, 2020, **142**, 14688–14701.

28 F. C. F. Marcos, L. Lin, L. E. Betancourt, S. D. Senanayake, J. A. Rodriguez, J. M. Assaf, R. Giudici and E. M. Assaf, Insights into the methanol synthesis mechanism via CO_2 hydrogenation over Cu-ZnO-ZrO_2 catalysts: Effects of surfactant/Cu-Zn-Zr molar ratio, *J. CO_2 Util.*, 2020, **41**, 101215.

29 D. Jiao, Y. Tian, Y. Liu, Q. Cai and J. Zhao, Vacancy-induced high activity of MoS_2 monolayers for CO electroreduction: A computational study, *Sustainable Energy Fuels*, 2021, **5**, 4932–4943.

30 J. Jia, Z. Chen, Y. Liu, Y. Li and J. Zhao, RuN_2 monolayer: A highly efficient electrocatalyst for oxygen reduction reaction, *ACS Appl. Mater. Interfaces*, 2020, **12**, 54517–54523.

31 X. Y. Zhang, W. J. Li, X. F. Wu, Y. W. Liu, J. Chen, M. Zhu, H. Y. Yuan, S. Dai, H. F. Wang, Z. Jiang, P. F. Liu and H. G. Yang, Selective methane electrosynthesis enabled by a hydrophobic carbon coated copper core-shell architecture, *Energy Environ. Sci.*, 2022, **15**, 234–243.

32 Y. Luo, Y. Cui, M. Li, X. Zhang, Y. Dai, C. Ling and Y. Huang, Density Functional Theory Investigation of Structure-Activity Relationship for Efficient Electrochemical CO_2 Reduction on Defective $SnSe_2$ Nanosheets, *ACS Appl. Nano Mater.*, 2021, **4**, 2760–2767.

33 N. Han, M. Sun, Y. Zhou, J. Xu, C. Cheng, R. Zhou, L. Zhang, J. Luo, B. Huang and Y. Li, Alloyed palladium-silver nanowires enabling ultrastable carbon dioxide reduction to formate, *Adv. Mater.*, 2021, **33**, e2005821.

This journal is © the Partner Organisations 2023

Inorg. Chem. Front., 2023, **10**, 168–173 | **173**